CHALMERS
UNIVERSITY OF TECHNOLOGY

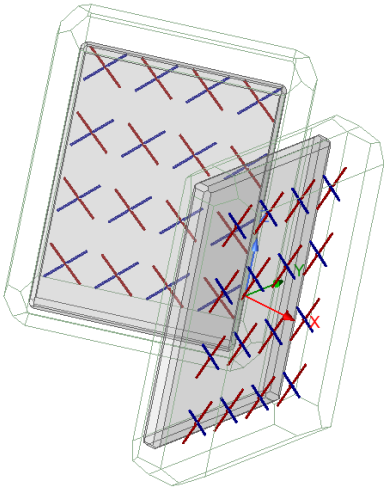

Automation of Antenna Isolation Modeling

Master's thesis in Information and Communication Technology

SRI SAI SATYANARAYANA DAMARAJU

DEPARTMENT OF ELECTRICAL ENGINEERING

CHALMERS UNIVERSITY OF TECHNOLOGY
Gothenburg, Sweden 2025
www.chalmers.se

Master's thesis 2025

Automation of Antenna Isolation Modeling

A Master of Science thesis in the Information and Communication Technology Master's Programme

SRI SAI SATYANARAYANA DAMARAJU

CHALMERS
UNIVERSITY OF TECHNOLOGY

Department of Electrical Engineering
Division of Communications, Antennas, and Optical Networks
Chalmers University of Technology
Gothenburg, Sweden 2025

Automation of Antenna Isolation Modeling
A Master of Science thesis in the Information and Communication Technology Master's Programme (MPICT)
SRI SAI SATYANARAYANA DAMARAJU

© SRI SAI SATYANARAYANA DAMARAJU, 2025.

Supervisor: Dr. Ola Tageman,
Expert mm-wave Integrated Sub-Systems,
Ericsson Research, Gothenburg, Sweden

Examiner: Prof. Dr. Jian Yang,
Communications, Antennas and Optical Networks Division,
Department of Electrical Engineering,
Chalmers University of Technology, Gothenburg, Sweden

Master's Thesis 2025
Department of Electrical Engineering
Chalmers University of Technology
SE-412 96 Gothenburg
Telephone +46 31 772 1000

Cover: Antenna design constructed in Ansys HFSS showing a 4x4 array separated with a 120-degree angle and isolation, and mutual coupling between elements.

Typeset in LaTeX
Printed by Chalmers Reproservice
Gothenburg, Sweden 2025

Automation of Antenna Isolation Modeling
SRI SAI SATYANARAYANA DAMARAJU
Department of Electrical Engineering
Chalmers University of Technology

Abstract

This thesis enhances an existing Python-based automation framework for antenna isolation modeling in large-scale antenna arrays, developed by Ericsson Research. The framework utilizes ANSYS HFSS via the PyAEDT API for automating electromagnetic workflows, enabling systematic variation of antenna array parameters including geometry, element spacing, polarization configurations, etc. which are loaded for model creation. This builds a complete 3D antenna array model in HFSS with proper excitation and boundary conditions, which then extracts comprehensive S-parameter data from simulation results and provides visualization capabilities with mathematical error metrics for evaluating mesh convergence and simulation reliability.

This work extends the framework with advanced performance evaluation and additional comparative analysis capabilities. Key contributions include the development of simulation performance evaluation tools that systematically analyze HFSS log files to extract information as resource utilization and convergence behavior, estimating error-free dynamic range and computational efficiency enabling quantitative comparison of simulation performance across different array configurations and computational runs. This is critical for optimizing simulation workflow and validating result accuracy in large-scale antenna modeling. Additionally, the extended framework provides comprehensive S-parameter comparison tools that perform quantitative analysis between different antenna simulations facilitating systematic evaluation of design variation and isolation performance characteristics.

Keywords: Antenna Isolation, HFSS Automation, Performance Evaluation, PyAEDT, S-Parameter Analysis.

Acknowledgements

First and foremost, I would like to express my deepest gratitude to Dr. Ola Tageman at Ericsson for his unwavering support, insightful guidance, and constructive feedback throughout the course of my thesis. Under his mentorship, I discovered the powerful capabilities of Python in the antenna field—an eye-opening experience that significantly shaped my work.

I am sincerely thankful to Dr. Parisa Aghdam at Ericsson for her pivotal role in facilitating this project; her leadership in ensuring access to necessary tools and her strategic guidance in resource management were instrumental to the seamless execution of my research. I am also grateful to Vinnova for their generous funding, which enabled this research and supported the pursuit of innovation with the potential for meaningful societal impact. Additionally, I extend my thanks to my colleagues at Ericsson for their valuable insights and camaraderie, as their diverse perspectives and collaborative spirit greatly enriched my research journey.

A special note of appreciation goes to Professor Dr. Jian Yang, my university supervisor, whose rigorous academic scrutiny and valuable feedback consistently pushed me to refine my hypotheses and elevate the quality of my analysis.

Lastly, my heartfelt thanks go to Rohith Virinchi. His constant encouragement and belief in me have been a source of strength and resilience throughout this academic endeavor. I am truly grateful for his presence and support during my thesis.

Sri Sai Satyanarayana Damaraju
Gothenburg
May 2025

List of Acronyms

Below is the list of acronyms that have been used throughout this thesis listed in alphabetical order:

AEDT	Ansys Electronics Desktop
API	Application Programming Interface
CCM	Convergence Cost Metric
COM	Component Object Model
CPU	Central Processing Unit
CST	Computer Simulation Technology
CSV	Comma-Separated Values
DDM	Domain Decomposition Method
E-field	Electric Field
EM	Electromagnetic
FEBI	Finite Element Boundary Integral
FEM	Finite Element Method
GPU	Graphics Processing Unit
GUI	Graphical User Interface
H-Field	Magnetic Field
HFSS	High Frequency Structure Simulator
HPC	High-Performance Computing
ISAC	Integrated Sensing and Communication
JSON	JavaScript Object Notation
MCA	Multiple Component Array
MIMO	Multiple-Input Multiple-Output
MoM	Method of Moments
PyAEDT	Python Ansys Electronics Desktop
RAM	Random Access Memory
SRD	Simulation Resource Density
S-parameter	Scattering Parameter
VSWR	Voltage Standing Wave Ratio
Z-parameter	Impedance Parameter

Nomenclature

Below is the nomenclature of indices, parameters, and variables that have been used throughout this thesis.

Indices

i,j	Indices for antenna array elements and S-parameter matrix positions
k	Index for frequency points
n	Index for mesh refinement passes

Parameters

ϵ	Small numerical value to prevent logarithmic singularities
λ	Wavelength at operating frequency [m]
ϕ_{ij}	Phase of S-parameter between ports i and j [rad]
θ	Array rotation angle [rad]
τ_g	Group delay [s]
ω	Angular frequency [rad/s]
d_x, d_y	Element spacing in x and y directions [m]
f	Frequency [Hz]
l	Dipole antenna length [m]
n_x, n_y	Number of array elements in x and y directions
N_{ports}	Total number of antenna ports
$N_{S-parameters}$	Total number of S-parameters in matrix
R_{rad}	Radiation resistance [Ω]
Z_0	Reference impedance (typically 50 Ω)

Variables

S_{ij}	Scattering parameter from port i to port j
$\|S_{ij}\|$	Magnitude of S-parameter
Z_{ij}	Impedance parameter between ports i and j [Ω]
$\Delta\|S_{ij}\|$	Change in S-parameter magnitude between mesh refinement passes
$e1$-$e6$	Error metrics for convergence analysis
VSWR	Voltage Standing Wave Ratio
$[I]$	Identity matrix
$[S]$	S-parameter matrix
$[Z]$	Z-parameter matrix
$\mathbf{P}_{final}$	Final position vector of antenna element after transformations [m]
$\mathbf{T}_{\text{center}}, \mathbf{T}_{\text{grid}}, \mathbf{T}_{\text{array}}$	Translation vectors for array positioning [m]
$\mathbf{R}_y(\theta)$	Rotation matrix about y-axis
$\mathbf{S}(f_k)$	S-parameter matrix at frequency point k

Contents

List of Figures

List of Tables

Listings

1

Introduction

1.1 Background

The rapid evolution of wireless communication systems has fundamentally transformed the requirements for antenna design and antenna analysis. Modern communication technologies such as full duplex communication, Integrated Sensing and Communication(ISAC), and antenna co-location scenarios will demand a sophisticated antenna arrays with hundreds or thousands of elements which are operating in a close proximity. Full duplex systems enable simultaneous transmission and reception on the same frequency with a requirement of stringent isolation between transmitting and receiving antennas to prevent self-interference [2]. Integrated Sensing and Communication (ISAC) systems combine radar sensing and communication functionalities, requiring careful electromagnetic isolation to preserve sensing accuracy and communication quality [3]. Co-location scenarios involve multiple antenna systems sharing limited installation space which require sufficient isolation to prevent mutual interference between different services.

Antenna isolation, to be defined as the electromagnetic decoupling between different antenna elements which has become a critical design parameter within wireless systems. Achieving adequate isolation will present a significant practical challenges due to its physical size constraints that limit separation distances which would make electromagnetic coupling inevitable. This would result in the complexity of accurately modeling large antenna arrays creating computational bottlenecks where each simulation can require hours or days of processing time limiting iterative design optimization.

Traditional approaches to antenna isolation analysis have largely relied on manual design process using electromagnetic simulation software through a graphical user interface(GUI). While this works well and provides accurate results for small-scale problems, its increasingly impractical as array sizes grows, as extensive repetitive modeling tasks, time-intensive parameter sweeps, and error-prone data extraction process of engineering effort for arrays containing all the elements. These challenges of manual modeling complexity, computational requirements, and computational analysis needs emphasize the critical requirement for automated workflows that can systematically generate models, execute simulations, and extract relevant performance data for analysis and comparison.

Recent developments in software automation frameworks, particularly the Python-Ansys Electronics Desktop(PyAEDT) interface for HFSS(High-Frequency Structure Simulator), have created new opportunities for addressing these challenges, which

enables programmatic control of electromagnetic simulation software to automating workflow. However, the effective implementation of such automation systems require careful consideration of software architecture, model parameterization strategies, and validation procedures.

1.2 Purpose and Goal

1.2.1 Purpose and Need for Automated Analysis

The analysis of antenna isolation in large-scale arrays presents significant practical challenges that extend beyond the electromagnetic complexity itself. Modern antenna arrays containing hundreds or thousands of elements generate thousands of S-parameters that must be systematically evaluated across multiple frequency points and configuration scenarios. For a typical dual-array system with 36 ports, each simulation produces 1,296 S-parameter relationships, requiring comprehensive analysis to extract meaningful design insights for isolation characterization.

Traditional manual approaches to such analysis involve repetitive modeling tasks through graphical user interfaces, time-intensive parameter sweeps, and complex data processing workflows. The iterative nature of antenna design compounds these challenges, as each design modification requires complete re-simulation including model creation, mesh generation, solution convergence, and post-processing analysis. For large antenna arrays, this manual workflow can require weeks of effort per design iteration, making systematic design optimization and comparative studies impractical within realistic project timelines.

Furthermore, validating simulation reliability becomes increasingly complex as array sizes grow. Evaluating computational efficiency, and ensuring solution accuracy across millions of S-parameters requires systematic analysis of simulation data. The manual interpretation of convergence metrics and performance characteristics across multiple simulation attempts introduces both time delays and potential for analysis inconsistencies, emphasizing the critical need for automated validation and comparison frameworks that can systematically process and evaluate simulation results.

1.2.2 Research Goal and Framework Enhancement

While electromagnetic simulation tools like HFSS provide powerful capabilities for antenna analysis, the manual approach to large-scale antenna array modeling presents significant bottlenecks that limit design efficiency and systematic optimization. An existing automation framework developed at Ericsson Research addresses the fundamental challenge of programmatic antenna array generation using PyAEDT, providing a solid foundation that enables systematic analysis of large antenna arrays through automated model creation and simulation execution.

Building upon this established framework, this thesis enhances the existing automation system to address gaps in simulation reliability assessment and performance evaluation. The primary goal focuses on developing comprehensive methods to evaluate simulation efficiency by quantifying the relationship between compu-

tational effort and achieved electromagnetic precision, enabling optimal resource allocation while maintaining sufficient solution accuracy.

This work addresses the following research questions: How can simulation accuracy be systematically estimated and validated for large antenna arrays? How can simulation efficiency be quantified by considering both electromagnetic precision and computational resource requirements? How can simulation performance be systematically compared between different modeling configurations to optimize computational approaches? How can S-parameters for two different model configurations be compared in detail to facilitate the evaluation of various model simplification attempts aimed at reducing simulation time? Through addressing these questions, the enhanced framework transforms from a basic automation tool into a comprehensive analysis platform that enables systematic antenna isolation studies while ensuring both computational efficiency and solution reliability.

1.3 Thesis Outline

The remainder of this thesis is organized as follows:

- **Chapter 2: Theoretical Background** establishes the fundamental concepts of antenna theory, computational electromagnetics, and automation approaches.
- **Chapter 3: Automated Antenna Array Modeling System** details the five-stage automation framework architecture, including antenna model parameterization, automated model generation using PyAEDT, array population algorithms, and HFSS configuration management for large-scale antenna arrays.
- **Chapter 4: Simulation Data Extraction** presents the data extraction methodology from HFSS simulation results, including model validation, multi-domain S-parameter processing, convergence analysis, and custom data storage architectures for electromagnetic simulation data.
- **Chapter 5: Data Analysis and Visualization Framework** describes the automated data processing system, S-parameter visualization methods, convergence analysis techniques, simulation performance evaluation, and Touchstone file analysis capabilities.
- **Chapter 6: Comparative Analysis and Performance Evaluation** outlines the systematic evaluation framework for multiple antenna array configurations, including electromagnetic parameter comparison methods, quantitative S-parameter difference analysis, and simulation performance benchmarking.
- **Chapter 7: Results** presents comprehensive case studiy and analyses of antenna array models processed through the automation framework, demonstrating isolation characteristics, computational performance metrics, and validation of the automated modeling approach.
- **Chapter 8: Conclusion and Future Scope** summarizes the key enhancements made to the existing automation framework and outlines future research directions.

2

Theoretical Background

This chapter establishes the theoretical background to understand the framework exploring fundamental concepts of antenna theory, computational electromagnetics and principles that form the basis for efficient antenna isolation analysis.

2.1 Antenna Fundamentals

An antenna is a transducer that converts electrical energy into ElectroMagnetic(EM) waves for transmission, or conversely converts electromagnetic waves into electrical energy for reception serving as a interface between guided waves in transmission lines and free-space electromagnetic waves enabling wireless communication across various distances and applications.

2.1.1 Antenna Types and Classification

Antennas can be broadly classified into several categories based on their physical structure and radiation characteristics. The primary classifications include:

- **Wire Antennas:** Include dipoles, monopoles, and loop antennas, representing the most fundamental antenna types due to their simple structure and well-understood radiation properties
- **Aperture Antennas:** Such as horn antennas and parabolic reflectors, which radiate electromagnetic energy through a defined aperture area
- **Microstrip Antennas:** Consist of metallic patches printed on dielectric substrates, widely used in modern communication systems due to their low profile and ease of integration
- **Reflector Antennas:** Employ curved conducting surfaces to focus electromagnetic energy, achieving high directional gain
- **Antenna Arrays:** Multiple antenna elements arranged in specific patterns to achieve enhanced performance characteristics

Among these categories, wire antennas and specifically dipole configurations form the foundation for understanding antenna arrays used in modern communication systems, where multiple elements work together to achieve enhanced performance characteristics.

2.1.2 Dipole and Cross-Dipole Antenna

The basic dipole antenna consists of two conducting elements separated by a small gap, typically fed at the center having a physical length $l = \lambda/2$, where the

current distribution follows a sinusoidal pattern with maximum current at the center and zero current at the ends. The radiation pattern exhibits a characteristic toroidal shape with maximum radiation perpendicular to antenna axis.

Whereas, a cross-dipole antenna extends the basic dipole by incorporating two orthogonal dipole elements positioned perpendicular to each other enabling dual-polarized operation where each dipole element can independently transmit or receive electromagnetic waves providing horizontal or vertical polarization, or alternatively ±45-degree slant polarizations depending on the orientation.

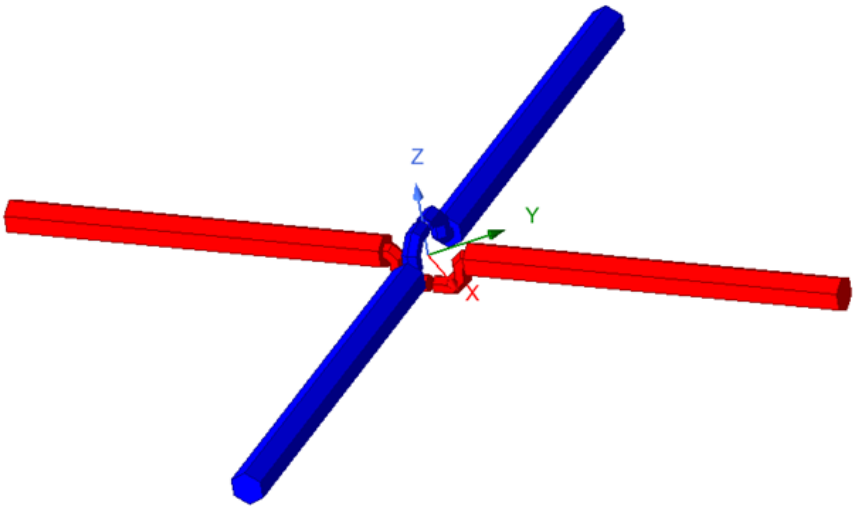

Figure 2.1: Cross-dipole antenna configuration showing orthogonal dipole elements perpendicular to each other.

The radiation resistance of a short dipole antenna (i.e., when the dipole length $l \ll \lambda$) can be approximated by[4]:

$$R_{rad} = 20\pi^2 \left(\frac{l}{\lambda}\right)^2 \ [\Omega] \tag{2.1}$$

where l is the dipole length in meters and λ is the wavelength in meters.

2.1.3 Antenna Performance Parameters

Understanding antenna performance requires the familiarity with several key parameters that characterize the electromagnetic behavior providing quantitative measure for antenna design optimization and system integration [4].

2.1.3.1 S-Parameters

S-parameters, or scattering parameters, describe the relationship between incident and reflected electromagnetic waves at antenna ports. For a two-port network, the S-parameter matrix relates input and output wave amplitudes:

$$\begin{bmatrix} b_1 \\ b_2 \end{bmatrix} = \begin{bmatrix} S_{11} & S_{12} \\ S_{21} & S_{22} \end{bmatrix} \begin{bmatrix} a_1 \\ a_2 \end{bmatrix} \tag{2.2}$$

where a_i represents incident wave amplitudes and b_i represents reflected wave amplitudes. The reflection coefficient S_{11} represents the ratio of reflected power to incident power at port 1, while S_{21} characterizes the transmission from port 1 to port 2.

S-parameters are complex quantities that can be represented in different forms:

- **Magnitude and Phase Representation:**

$$S_{ij} = |S_{ij}|e^{j\phi_{ij}} \tag{2.3}$$

  where $|S_{ij}|$ is the magnitude (dimensionless) and ϕ_{ij} is the phase in radians.
- **Real and Imaginary Representation:**

$$S_{ij} = \mathrm{Re}(S_{ij}) + j\mathrm{Im}(S_{ij}) \tag{2.4}$$

  where $\mathrm{Re}(S_{ij})$ and $\mathrm{Im}(S_{ij})$ are the real and imaginary components (dimensionless).

The conversion between (magnitude/phase) and (real/imaginary) forms follows:

$$|S_{ij}| = \sqrt{[\mathrm{Re}(S_{ij})]^2 + [\mathrm{Im}(S_{ij})]^2} \tag{2.5}$$

$$\phi_{ij} = \arctan\left(\frac{\mathrm{Im}(S_{ij})}{\mathrm{Re}(S_{ij})}\right) \ [\mathrm{rad}] \tag{2.6}$$

S-parameters are typically expressed in decibels for magnitude representation:

$$S_{ij} \ [\mathrm{dB}] = 20\log_{10}|S_{ij}| \tag{2.7}$$

When S-parameters are given in real and imaginary form, the magnitude must first be calculated before conversion to decibels, while the phase is expressed in degrees as:

$$\phi_{ij} \ [\mathrm{deg}] = \frac{180}{\pi}\arctan\left(\frac{\mathrm{Im}(S_{ij})}{\mathrm{Re}(S_{ij})}\right) \tag{2.8}$$

2.1.3.2 Z-Parameters

Z-parameters describe antenna impedance characteristics through the impedance matrix relating voltages and currents:

$$\begin{bmatrix} V_1 \\ V_2 \end{bmatrix} = \begin{bmatrix} Z_{11} & Z_{12} \\ Z_{21} & Z_{22} \end{bmatrix} \begin{bmatrix} I_1 \\ I_2 \end{bmatrix} \tag{2.9}$$

where V_i represents port voltages in volts [V], I_i represents port currents in amperes [A], and Z_{ij} represents impedance elements in ohms [Ω].

Z-parameters are complex quantities that can be calculated from S-parameters using conversion relationships. For a general N-port network with characteristic impedance Z_0, the conversion follows:

$$[Z] = Z_0([I] + [S])([I] - [S])^{-1} \tag{2.10}$$

where $[I]$ is the identity matrix, $[S]$ is the S-parameter matrix, and $[Z]$ is the Z-parameter matrix, Z_0 is the reference impedance, typically 50 Ω for antenna measurements.

2.1.3.3 Return Loss

Return loss quantifies the power reflected from an antenna port relative to the incident power, expressed as:

$$\text{Return Loss [dB]} = -20 \log_{10} |S_{11}| \tag{2.11}$$

A well-matched antenna exhibits high return loss values, indicating efficient power transfer and minimal reflection.

2.1.3.4 Voltage Standing Wave Ratio (VSWR)

VSWR describes the impedance mismatch between the antenna and transmission line:

$$\text{VSWR} = \frac{1 + |S_{11}|}{1 - |S_{11}|} \tag{2.12}$$

VSWR is dimensionless, with ideal matching corresponding to VSWR = 1 and practical systems typically requiring VSWR < 2.

2.1.3.5 Group Delay

Group delay characterizes the frequency-dependent phase response of antennas. Variations in such can cause signal distortion in communication systems.

$$\tau_g = -\frac{d\phi}{d\omega} \text{ [s]} \tag{2.13}$$

where ϕ is the phase in radians and ω is the angular frequency in rad/s.

2.1.4 Antenna Arrays and Element Spacing

Antenna arrays consist of multiple antenna elements arranged in a specific geometric patterns to achieve a desired radiation characteristics which couldn't be obtained with single-element antennas offering other advantages like increased directional gain, beam steering and improved spatial selectivity through constructive or destructive interference of electromagnetic fields. The fundamental principle of array operation is that EM waves from individual elements within, combine in space creating enhanced radiation in desired directions enabling higher gain, better directivity for modern communication systems[6].

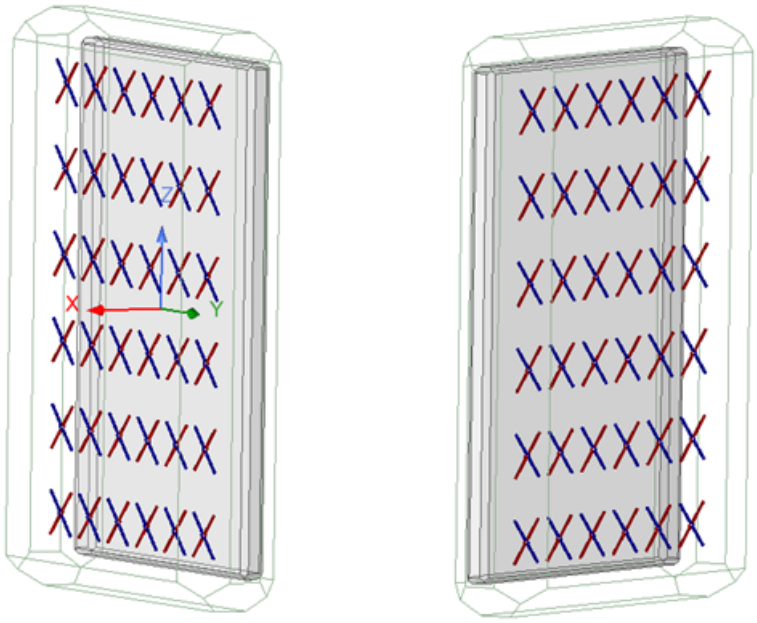

Figure 2.2: Rectangular antenna array geometry showing element spacing for $6 \times 6 + 6 \times 6$ configuration with coordinate system.

Other important design parameter is the spacing between array elements that directly affects the array performance. Element spacing is usually expressed in terms of wavelengths and significantly influences radiation pattern characteristics, mutual coupling levels. and overall array efficiency. From figure 2.2, rectangular arrays arrange elements in rows and columns with uniform spacing in both horizontal and vertical directions as per the array size. Maintaining proper spacing selection prevents unwanted radiation lobes(grating lobes) while maintaining acceptable coupling between adjacent elements.

The relationship between element spacing and array performance establishes fundamental design trade-offs in antenna engineering. While closer spacing reduces grading lobes and enables wider scan angles but increases mutual coupling between elements that can degrade individual element performance, conversely larger spacing reduces coupling effects but may introduce grating lobes that created unwanted radiation directions reducing the array efficiency. Modern array designs are to be carefully balancing these competing requirements while also considering other practical constraints.

2.1.5 Mutual Coupling in Antenna Arrays

Mutual coupling refers to the electromagnetic interaction between adjacent antenna elements within array configuration. This phenomenon occurs when the electromagnetic field radiated by one element induces currents in neighboring elements affecting the impedance and radiation characteristics. The coupling strength depends on several factors such as element spacing, antenna geometry, operating frequency, etc. The operating frequency affects coupling through wavelength-dependent near-field interactions. While mutual coupling typically involves near-

neighbor interactions, in the context of this work, the focus is on long-range coupling effects between separate arrays.

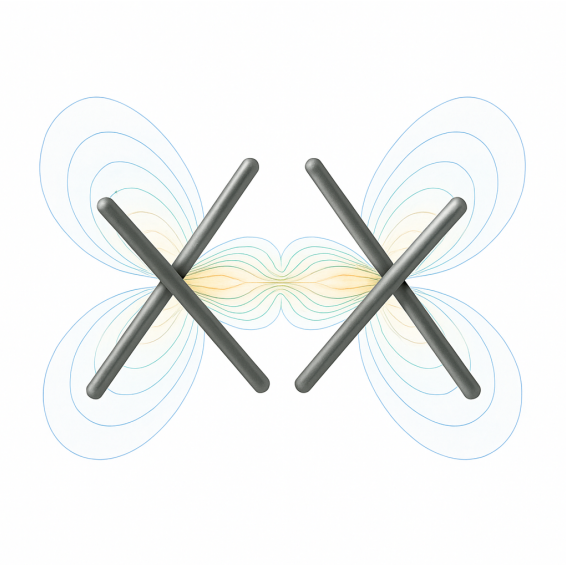

Figure 2.3: Mutual coupling illustration between two antenna elements showing electromagnetic field interaction and induced currents[5].

The effects of mutual coupling include impedance variations across array elements, altered radiation patterns, and reduced antenna efficiency. In communication systems, excessive mutual coupling can lead to signal correlation, reduced spatial diversity, and compromised system capacity. Understanding and controlling mutual coupling is essential for optimizing antenna array performance in practical applications[6].

2.2 Computational Electromagnetics Methods

When faced with real-world antenna problems, we quickly discover that Maxwell's equations, while elegant and complete, become nearly impossible to solve analytically for anything beyond the simplest geometries. Consider trying to calculate the radiation pattern of a smartphone antenna surrounded by a metal case, or determining how closely we can place antenna elements in an array before mutual coupling becomes problematic. These practical questions require numerical solutions because the mathematical complexity exceeds what can be handled with pencil and paper.

Computational electromagnetics provides the bridge between electromagnetic theory and practical antenna design. Rather than attempting to find exact analytical solutions, these methods break down complex problems into smaller, manageable pieces that computers can solve numerically. Think of it as solving a large jigsaw puzzle by working on small sections at a time, then assembling the complete picture.

The fundamental approach involves converting Maxwell's differential equations into systems of algebraic equations that computers can solve efficiently. This transformation process, called discretization, represents continuous electromagnetic fields

using discrete values at specific points or over small regions in space. Different computational methods employ various discretization strategies, each with particular strengths and limitations depending on the problem characteristics.

2.2.1 Finite Element-Boundary Integral (FEBI) Method

The Finite Element-Boundary Integral (FEBI) method represents a powerful hybrid approach that combines geometric flexibility of FEM with computational efficiency of Boundary Integral techniques for open-region electro-magnetics addressing the limitations of individual methods by utilizing finite elements to model complex geometries and material properties within near-field region, while employing boundary integral equations to handle radiation and scattering in the unbounded far-field region. This method is particularly well-suited for antenna and array analysis, where accurate modeling of both detailed antenna structures and radiation into free space is essential.

FEBI divides the computational domain into two regions: an inner finite element region containing the antenna structures, and an outer region extending to infinity that is handled using boundary integral formulations. By doing such, this eliminates the need of artificial absorbing boundaries providing accurate solutions for radiation problems while maintaining computational efficiency, make it an attractive choice for large-scale antenna array simulations. For the same, this method has become a standard approach in commercial electromagnetic simulation software for antenna design and analysis applications[7]. However, this method can experience convergence difficulties when dealing with electrically large structures with high mutual coupling, requiring careful mesh generation and solver parameter optimization.

2.3 HFSS Software and Modeling

ANSYS HFSS (High Frequency Structure Simulator) represents a comprehensive electromagnetic simulation environment that implements the finite element method to solve Maxwell's equations in three-dimensional structures. Understanding how this software operates and its modeling capabilities provides insight into practical electromagnetic analysis workflows and the computational implementation of the theoretical concepts discussed in previous sections.

Rather than requiring users to implement complex mathematical formulations manually, HFSS provides an integrated environment where electromagnetic problems can be set up, solved, and analyzed through a combination of graphical interfaces and programmatic controls. The software handles the underlying mathematical complexity while allowing users to focus on problem definition, geometry creation, and results interpretation [8].

2.3.1 Multiple Component Arrays in HFSS

When analyzing antenna arrays, the repetitive nature of array elements suggests that computational efficiency could be improved by avoiding redundant calculations. HFSS addresses this through its Multiple Component Array (MCA) functionality,

which leverages the similarity between array elements to reduce both modeling complexity and computational requirements.

Multiple Component Array Concept

The MCA approach recognizes that identical array elements will have identical electromagnetic characteristics when placed in identical environments. By defining a single element as a reusable component, the software can replicate this element across the array geometry while maintaining proper electromagnetic coupling between elements [8].

Figure 2.4: HFSS Array Tool interface demonstrating multiple component array configuration for systematic antenna array modeling.

As illustrated in Figure 2.4, the Array Tool interface provides systematic controls for array generation and management. The interface allows specification of array dimensions, element spacing, and excitation patterns through structured parameter entry rather than manual element-by-element definition.

Current Implementation Considerations

While the MCA functionality offers clear advantages for array analysis, its implementation requires careful consideration of computational resources and analysis objectives. The initial setup and validation of component definitions may require substantial effort to ensure that the simplified model accurately represents the intended array behavior.

Due to time constraints in the current work, the MCA approach was not explored for the array analyses presented in this study. Instead, individual element modeling was employed to maintain full control over the analysis process and to ensure that all electromagnetic interactions were explicitly captured without relying on software-specific optimization techniques.

Future work could explore the MCA capabilities more thoroughly, particularly for large array analyses where computational efficiency becomes a limiting factor. The potential benefits in terms of reduced modeling time and computational require-

ments make this approach attractive for extensive parametric studies or optimization investigations.

2.4 Automation in Electromagnetic Modeling

The increasing complexity of modern electromagnetic systems has created a significant demand for automation in simulation workflows. Traditional electromagnetic modeling approaches rely heavily on manual processes through graphical user interfaces, which become increasingly time-consuming and error-prone as system complexity grows. For large-scale antenna arrays containing hundreds or thousands of elements, manual model creation, parameter sweeping, and data extraction can require weeks or months of engineering effort. This limitation has driven the development of automated simulation frameworks that can systematically generate models, execute simulations, and process results without extensive human intervention.

Automation in electromagnetic modeling encompasses various aspects including model generation, batch simulation execution, systematic data extraction, and automated result analysis. Modern automation frameworks define simulation templates and parameter sets that can be automatically instantiated across multiple design variations. These systems can execute complex design space explorations, perform statistical analysis, and generate comprehensive reports without manual oversight. The automation approach not only reduces simulation time and human effort but also improves result consistency and enables the generation of large datasets necessary for advanced analysis techniques. Furthermore, automated workflows facilitate integration with optimization algorithms and design exploration tools, creating comprehensive design environments that can systematically improve antenna performance.

2.4.1 PyAEDT Interface for HFSS

PyAEDT represents a comprehensive Python interface that provides programmatic access to ANSYS Electronics Desktop (AEDT) applications including HFSS. This interface enables to control HFSS functionality through python scripts for automated model creation, execution, and post-processing operations. PyAEDT reduces the complexity of HFSS native scripting language while providing complete access to the full range of software capabilities including geometry creation, material assignment, boundary condition specification , mesh control and solver configuration.

The power of PyAEDT is demonstrated through its ability to create complex geometries with minimal code. For example, a simple dipole antenna can be generated using the following Python script[9]:

```
from pyaedt import Hfss
hfss = Hfss(specified_version="2024.2",
            non_graphical=False,
            new_desktop_session=True)

arm_length = 1
gap = 0.2
radius = 0.2
```

```
9
10 hfss.modeler.create_cylinder(cs_axis="Z",
11                               position=[0, 0, gap/2],
12                               radius=radius,
13                               height=arm_length)
14
15 hfss.modeler.create_cylinder(cs_axis="Z",
16                               position=[0, 0, -gap/2 - arm_length],
17                               radius=radius,
18                               height=arm_length)
```

Listing 2.1: PyAEDT script for creating a simple dipole antenna

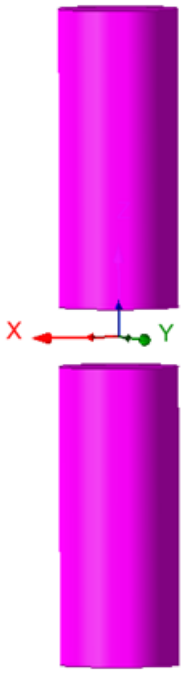

Figure 2.5: Simple dipole antenna geometry created using PyAEDT script showing the programmatic modeling.

The integration between pyAEDT and HFSS operate through the Component Object Model(COM) interface, allowing python scripts to communicate directly with the HFSS engine. As demonstrated in Listing 2.1 and Figure 2.5, which enables seamless automation of complex simulation workflows. PyAEDT provides object-oriented programming structures that mirror HFSS functionality, make it intuitive with electromagnetic modeling concepts supporting both local and remote simulation execution, enabling integration with high-performance computing resources and cluster environments.

2.4.2 Advantages of Programmatic Approach over Traditional GUI Methods

The programmatic approach to electromagnetic simulation offers substantial advantages over traditional GUI-based workflows, particularly for complex and repetitive modeling tasks. These advantages become increasingly significant as system complexity and analysis requirements grow:

- **Scalability and Efficiency:** Automated scripts can generate large-scale models and execute extensive parameter sweeps without manual intervention and later processing large amounts of data after simulation.
- **Consistency and Reproducibility:** Programmatic workflows eliminate human errors and ensure identical modeling approaches across different designs, providing consistent and reproducible results essential for comparative analysis.
- **Integration Capabilities:** Programmatic interfaces enable seamless integration with external tools including optimization algorithms, statistical analysis packages, and machine learning frameworks, creating comprehensive design environments.
- **Parametric Design Exploration:** Automated frameworks can systematically explore large design spaces through parametric sweeps and sensitivity analysis, identifying optimal configurations that might be missed through manual approaches.
- **Batch Processing and Parallelization:** Scripts can distribute simulations across multiple computing resources and execute batch processing operations, significantly reducing overall analysis time for complex projects.

These advantages make programmatic approaches essential for modern electromagnetic design workflows, where traditional GUI methods become limiting factors in achieving comprehensive analysis and optimization of complex antenna systems.

Confidentiality Notice

Confidentiality Agreement

As per Ericsson confidentiality Agreement, the information communicated in conjunction with the Assignment for Ericsson and that is not already generally known through publication shall be treated as being confidential and shall not be disclosed for any other purpose.

Under this agreement:

Chapters 3, 4, 5, 6

are not disclosed for public preview

7
Results

This chapter presents the comprehensive results obtained from the enhanced automation framework for antenna isolation modeling demonstrating framework's capabilities across the complete workflow (starting from Model generation to Model Compare).

7.1 Testing Environment and Software Configuration

The automation framework was developed and tested using testing environment consisted of the following software versions:

- **Python:** Version 3.11.1
- **ANSYS HFSS:** Version 2024.2
- **PyAEDT:** Version 0.15.3

7.2 Automated Model Creation Result

The automated model creation process utilizes a comprehensive set of parameters. This section presents the specific parameter configuration used for generating the test case: **"Dipole Array, Rev 15_2, 3x3+3x3, AntArr - 8236"** as follows:

Table 7.1: Antenna Array Configuration Parameters for Test Case: AntArr - 8236

Parameter Category	**Configuration Details**
Array Geometry and Structure	
Array Configuration	Dual array system (single_array = False)
Array Dimensions	3×3 + 3×3 configuration (nx1=3, ny1=3, nx2=3, ny2=3)
Total Elements	18 antenna elements (9 elements per array)
Total Ports	36 ports (2 polarizations per element)
Element Type	Cross-dipole antennas with dual polarization capability
Spatial Positioning and Orientation	
Horizontal Separation	2 wavelengths (xseparation = 2)
Vertical Separation	0 wavelengths (yseparation = 0)
Angular Orientation	120-degree separation (yangle = '120deg')

Table 7.1 – continued from previous page

Parameter Category	**Configuration Details**
Reference Radius	6 wavelengths (radius = 6)
Positioning Mode	Normalized positioning (=True)
Excitation and Polarization Configuration	
Polarization Type	Horizontal linear polarization
Excitation Element	Center element of Array 1 (Element_1_5)
Source Configuration	Dual-port excitation (X and Y polarizations)
Element Distribution Mapping	
Array 1 Buildmap	All active elements (buildmap1.all_active)
Array 2 Buildmap	All active elements (buildmap2.all_active)
Active Elements	Full electromagnetic participation with X and Y ports
Load/Lumped/Void Elements	Not utilized in this configuration
Frequency and Analysis Parameters	
Reference Frequency	3.5 GHz (fref = 3.5e9)
Frequency Range	3.15 - 3.85 GHz (fstart = 3.15, fstop = 3.85)
Frequency Points	15 discrete points (fpoints = 15)
Mesh Frequency	3.5 GHz optimization
Element Spacing	Wavelength-normalized based on reference frequency
Simulation Accuracy and Solver Configuration	
Speed Level	Level 3 (balanced approach for most simulations)
Maximum Passes	6 adaptive refinement iterations
Solver Type	FEBI
Template and Component Configuration	
HFSS Template	DAP15_2_template_for_GDP16 (dual array)
Project File	Dipole Array, Rev 15_2.aedt
Active Components	GDP16.a3dcomp (cross-dipole elements)
Component Parameters	Predefined geometry and design variables

This parameter configuration generates a representative dual-array antenna system from framework as follows:

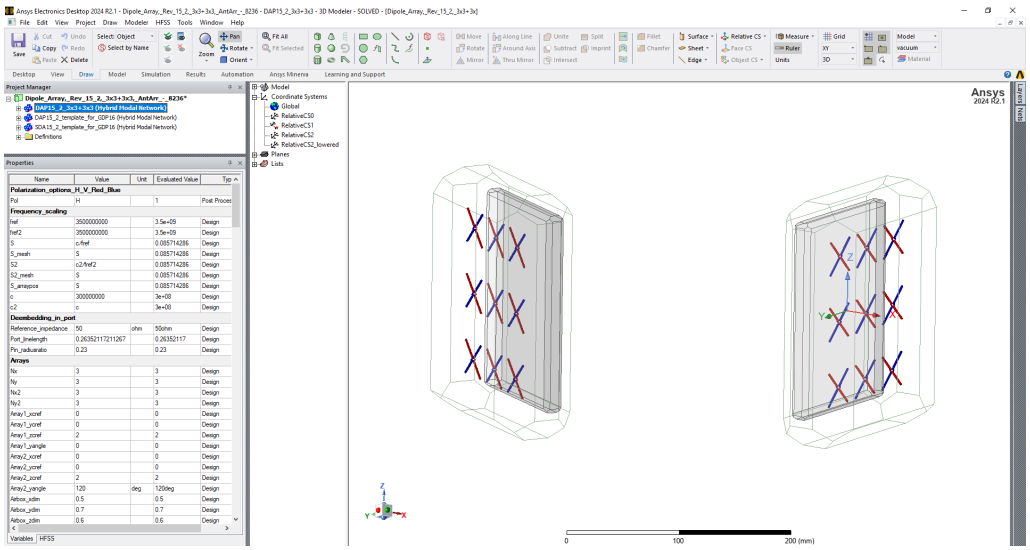

Figure 7.1: Generated 3D model of Dipole Array, Rev 15_2, 3×3+3×3, AntArr - 8236 as Table 7.1

7.3 Data Extraction Results

The data extraction process follows the methodology, systematically retrieving S-parameter data from HFSS simulation results and processing them into structured formats.

The following listings demonstrate a small part of extracted data formats(JSON and sNp) for the test case "AntArr - 8236":

```
"data_freq": {
    "discrete_sweep": {
        "extractmap_inter_1sparse_2sparse": {
            "convention": "Element_array(1 or 2)_elementnumber(
row first)_polarization(X-red-neg45 or Y-blue-pos45)",
            "imagdata": [
                {
                    "entry_key": S(Element_1_1_X,Element_2_1_X)
                    "freq_entries": [
                        {
                            "freq": 3.15,
                            "imag": 0.000845538476039103
                        },
                        {
                            "freq": 3.2,
                            "imag": 0.0005797380915756188
                        },
                        {
                            "freq": 3.4,
                            "imag": -0.0010324536887846751
                        },
```

```
                                {
                                    "freq": 3.85,
                                    "imag": -0.00047922947472753063
                                }
```

Listing 7.1: Sample JSON data structure showing extracted S-parameter imaginary components

```
! Touchstone file exported from HFSS 2024.2.1
!        File:           R:/HFSS from cluster/64159/Dipole_Array,_Rev_15_2,_3x3+3x3,_AntArr_-_8236.aedt
!        Generated:      12:24:28 AM May 24, 2025
!        Design:         DAP15_2_3x3+3x3
!        Project:        Dipole_Array,_Rev_15_2,_3x3+3x3,_AntArr_-_8236
!        Setup:          Setup1
!        Solution:       SweepDiscrete
# GHz S MA R 50.000000
! Terminal data exported
3.15  0.400810440579014 -36.7120325159593 0.0432075134977711 -147.267869696324 0.0874160468592595 89.217237227437 0.0663313140287666 -178.956574450542
  0.0156699220218193 -133.441081717354 0.0224999127213456 -27.042240243007 0.185876796156664 136.276584386435 0.14423257176528 34.0936740973737
  0.0376144844528315 122.813646107233 0.0145951865617113 115.324285156829 0.0131667545314536 -99.6345285627282 0.0122167328767924 -69.7332183776987
```

Listing 7.2: Sample Touchstone file header and data showing industry-standard S-parameter format

7.4 JSON Data Analysis and Visualization Results

The JSON data analysis and visualization results demonstrate the comprehensive analytical capabilities of the enhanced framework, following the methodologies.

7.4.1 S-Parameter Frequency Response Analysis

Figure 7.2 presents the frequency-domain S-parameter analysis using the discrete sweep data extracted from HFSS simulation, plotting S-parameter magnitudes in decibels across the 3.15-3.85 GHz frequency range for the inter-array sparse coupling map (extractmap_inter_1sparse_2sparse). Each trace represents electromagnetic coupling between elements in arrays which demonstrates the isolation characteristics of dual-array configuration with variations across the bandwidth, where stronger couplin (higher magnitude values) occur at specific frequencies due to the resonance effects and EM interactions between arrays which are positioned at 120-degree angular separation.

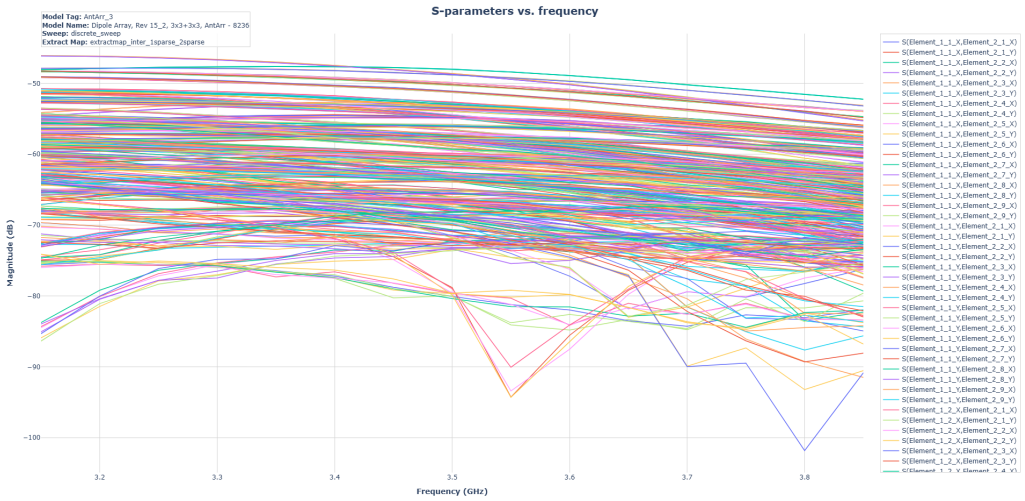

Figure 7.2: S-parameter magnitude versus frequency showing electromagnetic coupling behavior across the 3.15-3.85 GHz range

7.4.2 S-Parameter Convergence Across Refinement Passes

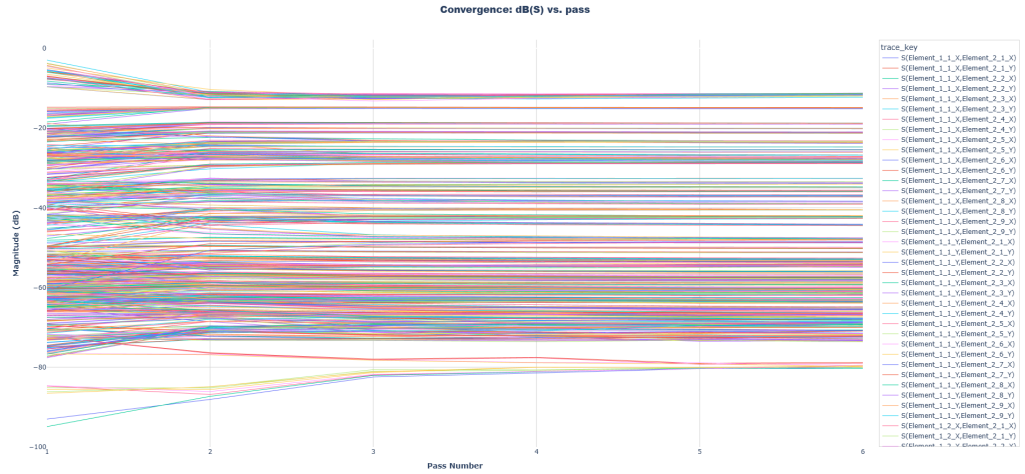

Figure 7.3: S-parameter magnitude convergence across adaptive mesh refinement passes showing solution stability

Figure 7.3 demonstrates the primary convergence visualization showing S-parameter magnitudes in decibels versus mesh refinement pass numbers. The plot reveals that most S-parameters stabilize after a initial refinement passes having minimal variations in subsequent iterations. This convergence behavior indicates successful adaptive mesh refinement, where the EM solution reaches stable values as finite element mesh is progressively refined capturing field gradients accurately.

7.4.3 Three-Dimensional Error Analysis

Figure 7.4 illustrates the 3D convergence metric, displaying the absolute convergence errors in 3D, as x-axis representing the final S-parameter coupling strength,

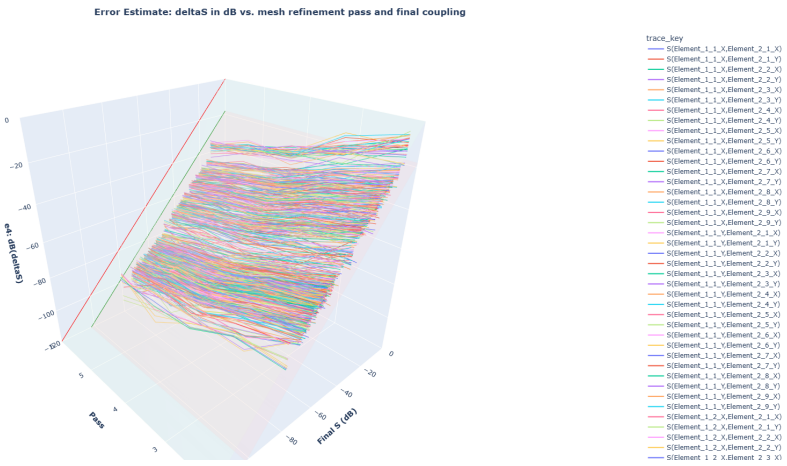

Figure 7.4: 3D visualization of absolute convergence errors (deltaS in dB) across mesh refinement passes and final coupling levels

y-axis shows the mesh refinement pass number, and the z-axis indicates the absolute delta-S magnitude in decibels. This visualization enables identification of systematic convergence patterns and reveals how different coupling levels behave during adaptive mesh refinement and reference lines 0 dB and -18 dB act as indicators for error assessment to identify which S-parameters require additional refinement passes to achieve acceptable accuracy.

7.4.4 Final Pass Convergence Assessment

Figure 7.5: Convergence check showing deltaS/S vs. final coupling strength with binned statistical analysis and reference thresholds

Figure 7.5 presents the final pass convergence assessment visualization methods. The plot combines raw scatter data (individual S-parameter convergence values) with a binned staircase representation that applies statistical smoothing using the

99th percentile within each magnitude bin. The horizontal reference line at -79 dB represents the 1dB-error range, meaning all the S-parameters weaker than -79 dB have converged to within 1 dB accuracy.

7.4.5 Basic Simulation Performance Analysis

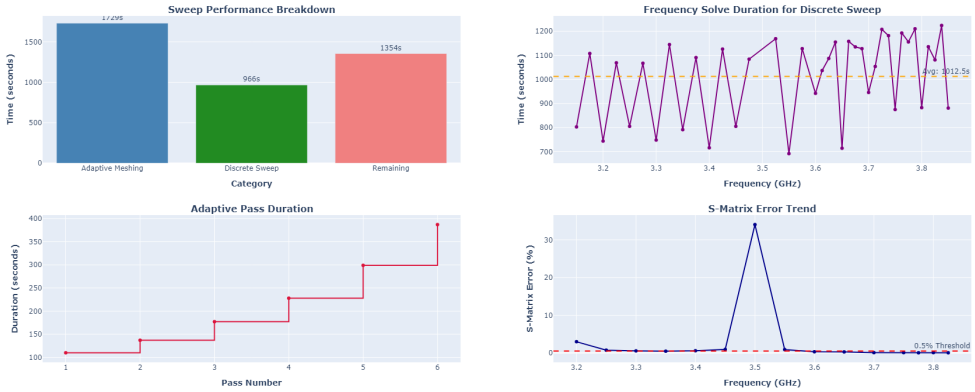

Figure 7.6: Basic simulation performance analysis showing time allocation, frequency solve duration, adaptive pass duration, and error trends

Figure 7.6 illustrates the fundamental performance characteristics extracted from the HFSS simulation log analysis. The analysis provides a comprehensive view of computational efficiency and convergence behavior across four key metrics:

- **Sweep Performance Breakdown (Subplot 1):** Time allocation analysis reveals that adaptive meshing consumes 1729 seconds, significantly exceeding the discrete sweep duration of 966 seconds, with remaining operations accounting for 1354 seconds. This distribution is characteristic of complex antenna array simulations where iterative mesh refinement dominates computational overhead, particularly for 36-port systems requiring high accuracy.
- **Frequency Solve Duration for Discrete Sweep (Subplot 2):** Individual frequency point processing times exhibit substantial variation across the 3.2-3.8 GHz range, with an average solve time of 1012.55 seconds per frequency point. The oscillating pattern between approximately 700-1200 seconds indicates frequency-dependent convergence complexity, where certain frequency points require additional computational effort due to resonance effects or field distribution complexity.
- **Adaptive Pass Duration (Subplot 3):** The step-wise progression shows increasing computational requirements for successive mesh refinement passes, escalating from approximately 110 seconds for Pass 1 to 390 seconds for Pass 6. This exponential growth pattern reflects the increasing mesh density and computational complexity as the adaptive algorithm refines critical regions to achieve the specified convergence criteria.
- **S-Matrix Error Trend (Subplot 4):** Convergence reliability assessment demonstrates generally stable error levels below the 0.5% threshold across most frequency points, with a notable exception at approximately 3.5 GHz where

the error exceeds 35%. This anomaly suggests potential convergence difficulties at this specific frequency, possibly indicating insufficient mesh density or numerical instabilities requiring additional refinement passes or modified solver settings.

7.4.6 Advanced Simulation Performance Metrics

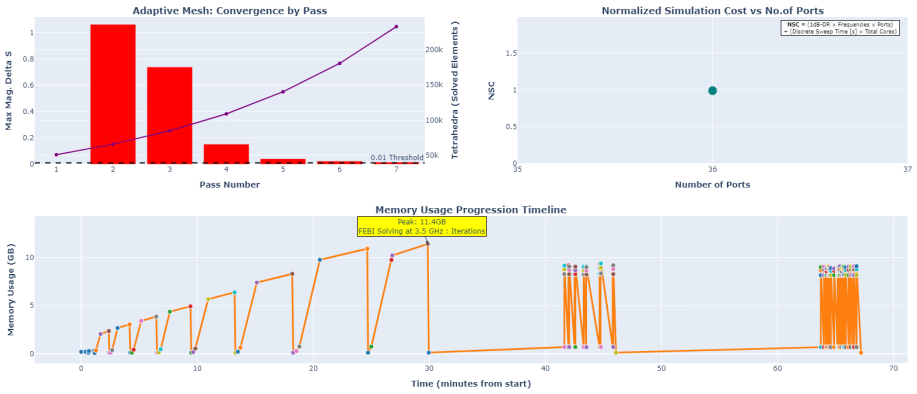

Figure 7.7: Advanced simulation performance metrics including adaptive mesh convergence analysis, normalized simulation cost, and memory usage progression

Figure 7.7 presents the advanced performance evaluation metrics extracted from comprehensive HFSS log file analysis, providing deeper insights into simulation efficiency and resource utilization:

- **Adaptive Mesh: Convergence by Pass (Subplot 1):** The convergence progression analysis shows the relationship between mesh refinement passes and achieved accuracy. The bar chart displays maximum magnitude Delta S values decreasing from 1.0 to approximately 0.15 across six adaptive passes, while the overlaid curve represents tetrahedral count growth reaching over 200k elements. The 0.01 threshold line indicates the target convergence criterion, demonstrating that convergence is achieved by Pass 4, with subsequent passes providing marginal accuracy improvements at significantly increased computational cost.
- **Normalized Simulation Cost vs No. of Ports (Subplot 2):** This scatter plot quantifies computational efficiency using the Normalized Simulation Cost (NSC) metric, calculated as the ratio of total computation time to the product of frequency points and port count. For the 36-port AntArr_1 configuration, the NSC value of approximately 1.0 indicates balanced computational efficiency relative to the problem complexity. This metric enables direct comparison between different antenna array configurations and guides optimization strategies for large-scale simulations.
- **Memory Usage Progression Timeline (Subplot 3):** The comprehensive memory utilization profile tracks resource consumption throughout the entire simulation workflow. Peak memory usage reaches 11.4GB during FEBI (Finite Element Boundary Integral) solving at 3.5 GHz iterations, as highlighted by

the yellow annotation box. The timeline reveals distinct phases: initial setup with minimal memory footprint, progressive memory allocation during adaptive meshing (0-25 minutes), peak utilization during frequency sweep solving (25-30 minutes), followed by memory deallocation and final processing phases (65-70 minutes). The multiple colored markers represent different simulation phases, enabling identification of memory bottlenecks and optimization opportunities for large antenna array simulations.

The advanced metrics collectively demonstrate that while the simulation achieves acceptable convergence levels, the significant memory requirements and extended processing times for frequency-dependent solving highlight the computational intensity inherent in high-fidelity antenna array modeling. These insights are crucial for scaling simulations to larger array configurations and optimizing computational resource allocation.

7.5 Touchstone File Analysis and Visualization Results

The Touchstone file analysis and visualization results demonstrate the framework's capabilities for processing industry-standard S-parameter data.

7.5.1 Return Loss Analysis

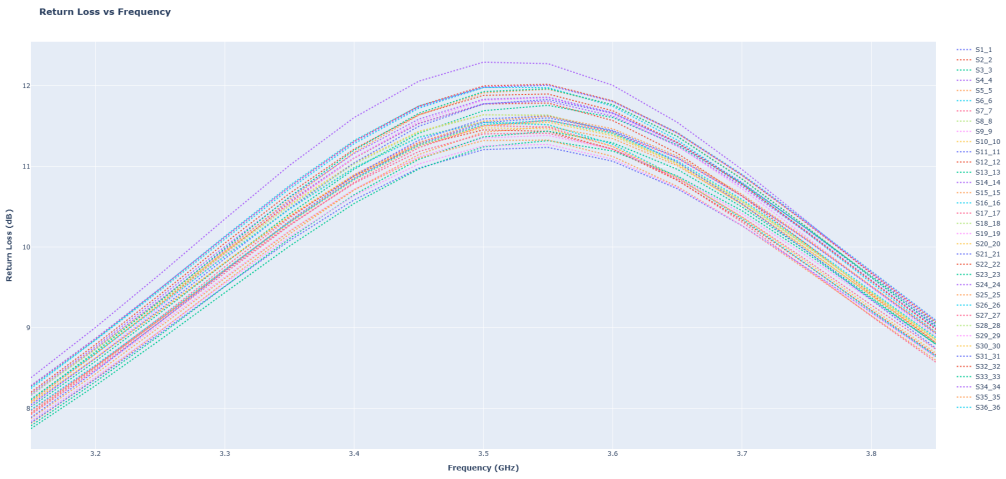

Figure 7.8: Return loss versus frequency for reflection coefficients showing impedance matching characteristics

Figure 7.8 illustrates the return loss characteristics calculated exclusively for diagonal S-parameters using equation (2.11). The plot shows return loss values ranging from approximately 8 to 12.5 dB across the frequency range. The curved response pattern with peak values around the center frequency indicates reasonable impedance matching at the design frequency of 3.5 GHz. Higher return loss values

(approaching 12-13 dB) suggest better matching, while the frequency variation reveals the bandwidth characteristics of the antenna elements within the dual-array configuration.

7.5.2 Group Delay Analysis

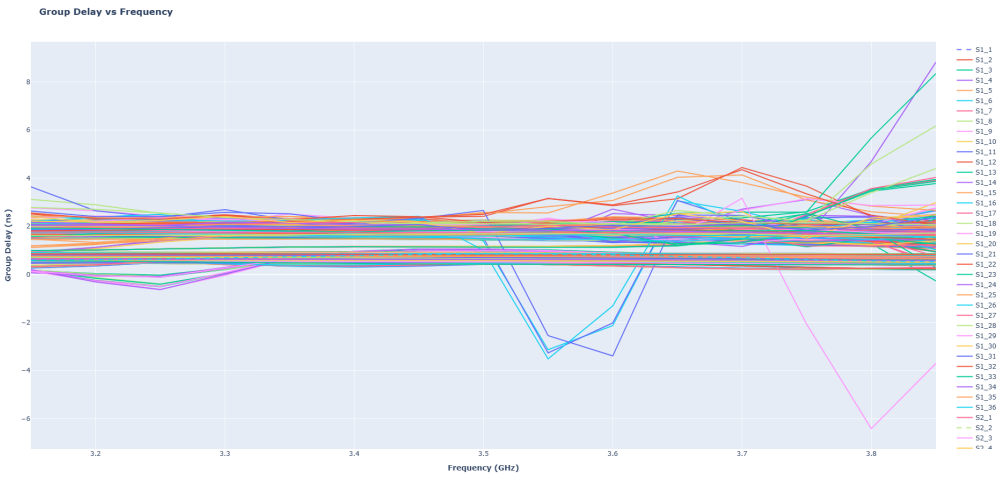

Figure 7.9: Group delay versus frequency showing phase linearity characteristics across the 3.15-3.85 GHz range

Figure 7.9 presents the group delay analysis computed using equation (2.13) through numerical differentiation of the phase response with phase unwrapping. The plot reveals the frequency-dependent phase response characteristics of the antenna array S-parameters. Most of the S-parameters do exhibit relatively stable group delay values between 0-4 nanoseconds across the frequency range indicating good phase linearity but some parameters do show significant variations particularly observed at higher frequencies within range that indicates a frequency-dependent phase distortion affecting signal integrity.

7.5.3 Three-Dimensional S-Parameter Visualization

Figure 7.10 presents the three-dimensional S-parameter visualization system that displays magnitude relationships across multiple dimensions, as x-axis representing frequency variation across the simulation bandwidth, the y-axis shows the magnitude at center frequency (3.5 GHz) providing a reference coupling level, and the z-axis represents the actual S-parameter magnitude in decibels. This plot enables identification of frequency-dependent coupling variations and assessment of how different S-parameters relate to each other across the operating bandwidth. The 3D representation reveals systematic patterns in electromagnetic coupling behavior, helping identify which parameter combinations exhibit similar frequency responses and coupling strengths relative to their center frequency reference values.

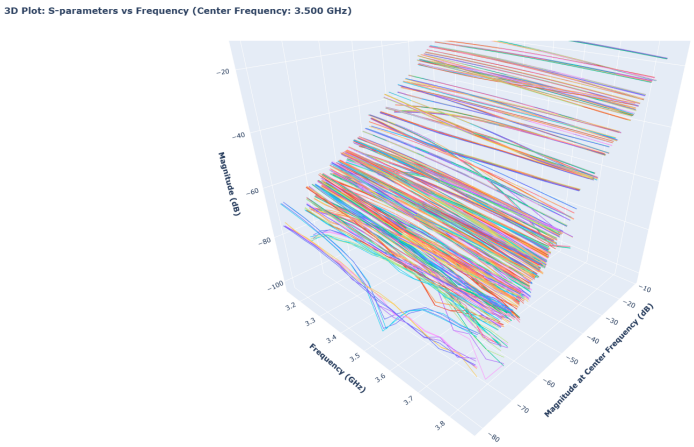

Figure 7.10: 3D visualization of S-parameters showing magnitude relationships across frequency and center frequency reference

7.5.4 Smith Chart Impedance Analysis

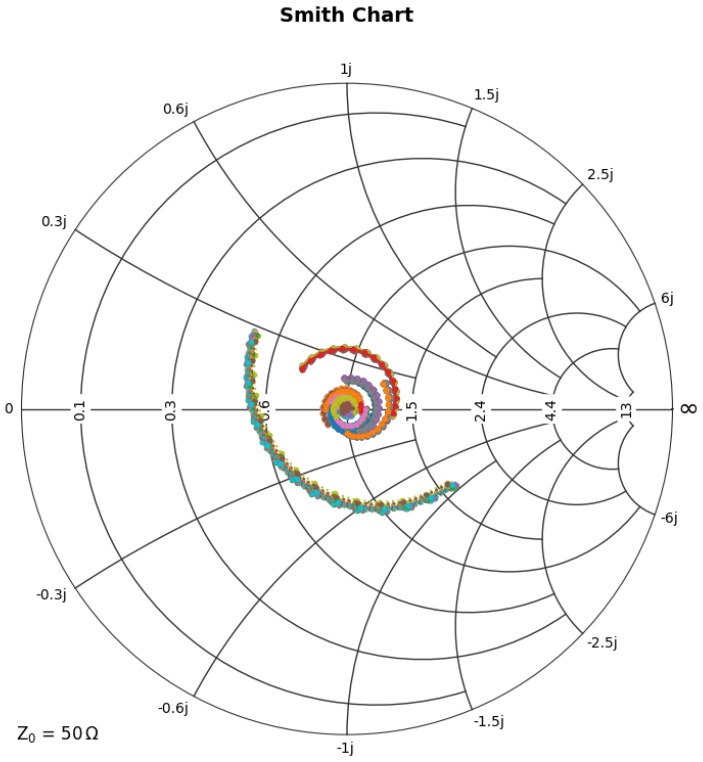

Figure 7.11: Smith chart visualization showing complex impedance characteristics at 50-ohm reference

Figure 7.11 provides impedance-based analysis through Smith chart visualization, transforming S-parameter data into complex representation. The plotted tra-

jectories show the frequency-dependent impedance behavior of S-parameters, with points near the chart center indicating good matching (low reflection) and points toward the periphery indicating impedance mismatches or reflection coefficients.

7.6 Comparative Analysis Results

The goal of the comparative analysis is to evaluate how two modeling approaches differ by examining all S-parameters. It serves two purposes: first, to visualize the differences through plots for easier troubleshooting; and second, to generate a single numerical score that summarizes the overall error across all S-parameters and frequencies. This score helps guide automated processes, such as adjusting simulations to balance accuracy and efficiency. A similar approach can be applied to NSC for consistent evaluation throughout multiple models. The following subsections present the comparative analysis results for AntArr_3 versus AntArr_4:

7.6.1 Return Loss and VSWR Comparison

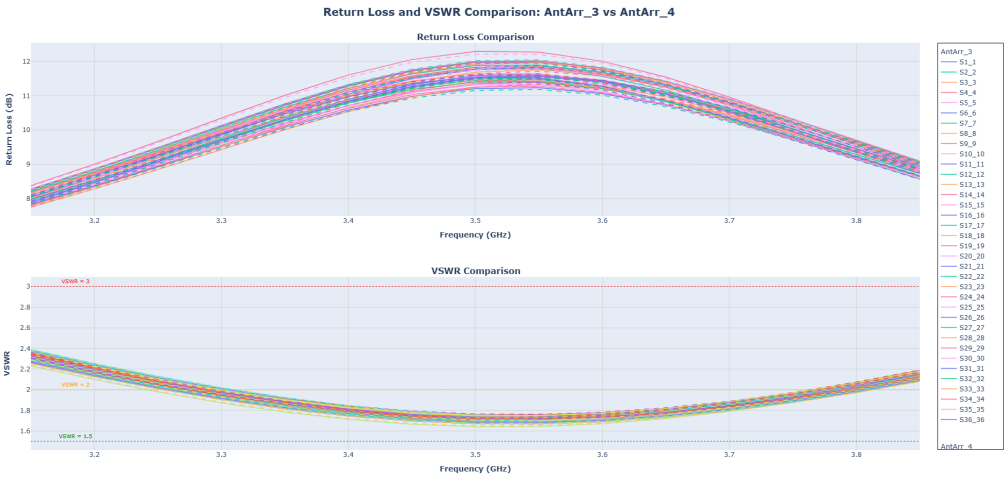

Figure 7.12: Return loss and VSWR comparison between AntArr_3 and AntArr_4 showing impedance matching characteristics

Figure 7.12 presents the return loss and VSWR analysis following the mathematical foundations. The upper subplot shows return loss comparison calculated, while the lower subplot displays VSWR characteristics computed using equation (2.12). Both antenna configurations exhibit similar return loss patterns ranging from 8-12 dB across the frequency band, with peak matching around 3.5 GHz. The VSWR comparison shows values between 1.5-2.5, with both configurations achieving VSWR < 2 around the center frequency, indicating acceptable impedance matching. The close agreement between the two configurations suggests consistent antenna design characteristics despite potential differences in array positioning or element variations.

7.6.2 Impedance Parameter Comparison

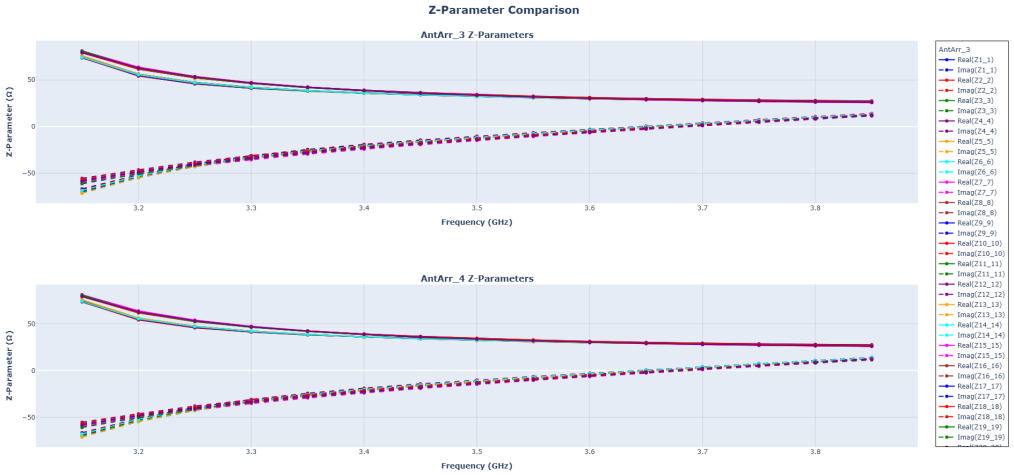

Figure 7.13: Z-parameter comparison showing complex impedance characteristics for both antenna configurations

Figure 7.13 illustrates the impedance parameter analysis following the Z-parameter. The plots show both real and imaginary components of diagonal Z-parameters (self-impedance characteristics) for both antenna configurations across the frequency range. AntArr_3 and AntArr_4 demonstrate very similar impedance behavior, with real parts ranging from approximately 20-80 ohms and imaginary parts varying from -60 to +20 ohms.

7.6.3 S-Parameter Coupling Heatmap Analysis

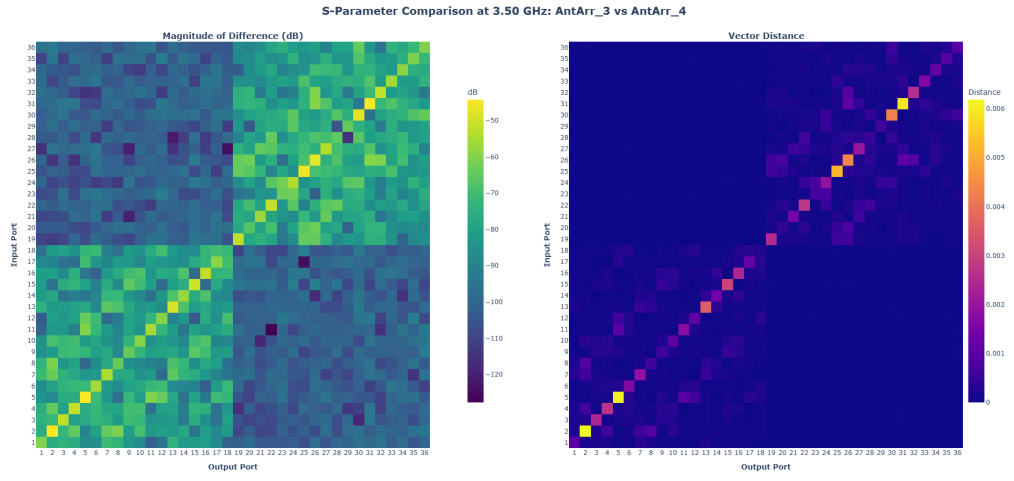

Figure 7.14: S-parameter coupling heatmap comparison showing magnitude differences and vector distances at center frequency

Figure 7.14 presents the heatmap-based coupling analysis, focusing on center frequency assessment at 3.5 GHz:

- **Magnitude Difference Heatmap (Left Subplot):** Shows the magnitude difference calculation, revealing variations ranging from -60 to 0 dB across the port matrix. Darker blue regions indicating smaller differences and lighter regions showing larger variations.
- **Vector Distance Heatmap (Right Subplot):** Displays the vector distance computation, providing linear-scale analysis showing distances up to 0.006 between complex S-parameters.

7.6.4 Maximum Relative Difference Assessment

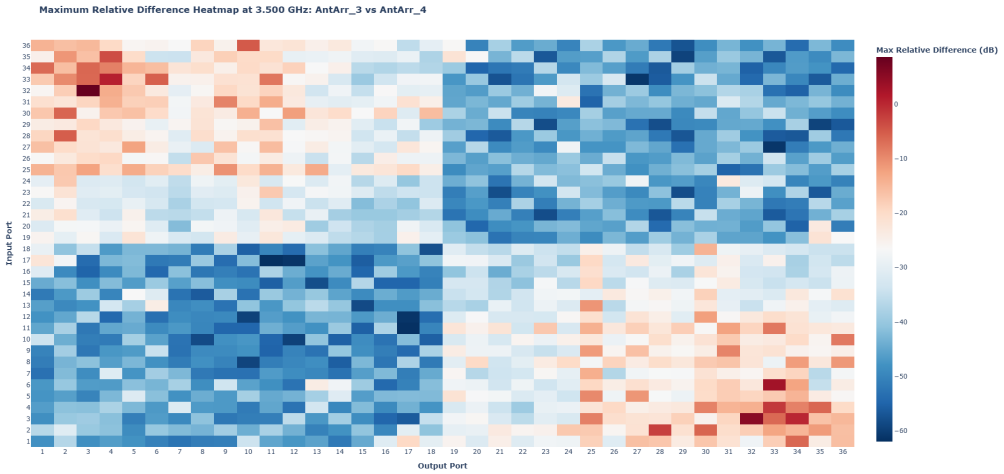

Figure 7.15: Maximum relative difference heatmap showing normalized coupling variations across the S-parameter matrix

Figure 7.15 illustrates the relative difference calculation, where S-parameter differences are normalized by the average magnitude to provide magnitude-independent assessment. The heatmap reveals systematic patterns related to the antenna array structure, with inter-array coupling elements (cross-block regions) showing different relative difference characteristics compared to intra-array coupling elements (diagonal blocks) enabling identification of which coupling paths exhibit the most significant variations between the two antenna configurations.

7.6.5 Three-Dimensional Relative Difference Visualization

Figure 7.16 presents the three-dimensional relative difference visualization extending the analysis across frequency and magnitude dimensions, where x-axis represents the average magnitude at center frequency, the y-axis shows frequency variation, and the z-axis displays the relative difference in decibels. This plot enables identification of frequency-dependent coupling variations and reveals how S-parameter differences vary with both coupling strength and frequency, showing that most relative differences cluster around -20 to -40 dB range, indicating good agreement between the two antenna configurations.

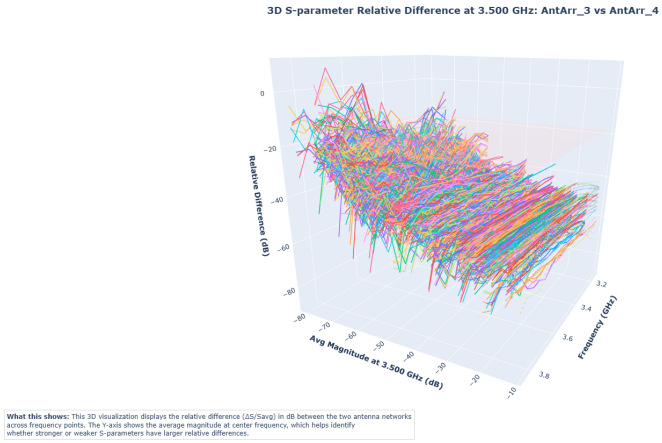

Figure 7.16: 3D visualization of S-parameter relative differences showing coupling variations across frequency and magnitude dimensions

7.6.6 Comparative sNp Relative Error Analysis

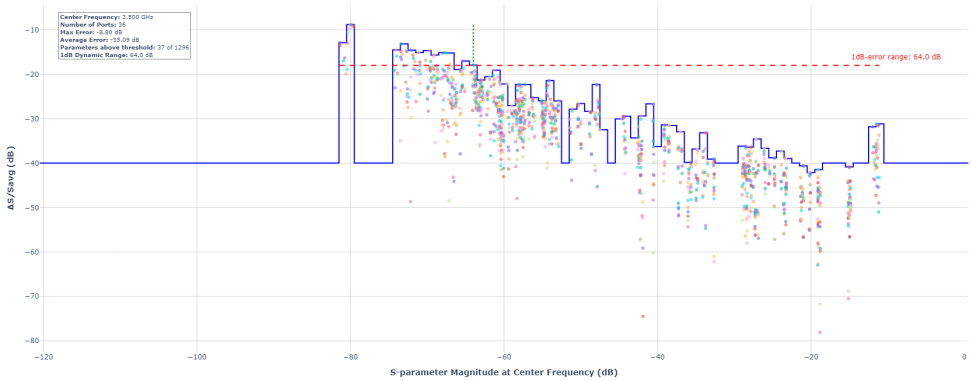

Figure 7.17: Comparative relative error analysis showing $\Delta S/S_{\text{avg}}$ vs S-parameter magnitude at 3.500 GHz

Figure 7.17 shows a relative error analysis comparing two antenna array configurations at 3.500 GHz across 36 ports. The analysis calculates the relative difference between the two designs and plots it against S-parameter magnitude to assess how well the two configurations agree with each other. The scatter plot shows that weaker S-parameters (those with lower magnitudes, e.g., below –40 dB) tend to have smaller absolute differences (ΔS) between the two antenna designs, but larger relative differences ($\Delta S/S$). This indicates that even small absolute changes in weak coupling paths can result in high relative variation.

The blue histogram overlay shows the distribution of relative errors across different S-parameter strength levels, with analysis revealing a maximum error of -8.60 dB and average error of -35.09 dB. With 37 out of 1296 total S-parameters exceeding the error threshold and a 1dB dynamic range spanning 64.0 dB, the results demonstrate good overall agreement between the two antenna configurations.

8

Conclusion and Future Scope

8.1 Conclusion

This thesis presents a collaborative effort with Ericsson research to extend an existing antenna array modeling framework into a comprehensive analysis platform. The work focused on enhancing simulation reliability, computational efficiency, and evaluation capabilities through three main areas: simulation accuracy analysis, touchstone file processing for S-parameter extraction, and comparative analysis between different antenna models. The existing approach involved analyzing the code base from Ericsson Research to understand modeling and data extraction mechanisms, which was then extended with new methods for simulation evaluation and comparative analysis.

The implementation addressed several technical challenges, particularly maintaining compatibility with the existing framework structure while introducing new analytical capabilities and correcting unforeseen complements in framework. The project successfully integrated touchstone file processing for detailed S-parameter analysis and developed tools to interpret simulation data in meaningful ways for practical antenna design decisions. While exploring the integration of multiple component arrays from HFSS showed promise as a potential simplification method, time constraints prevented full implementation of this approach into the framework, leaving it as a foundation for future development. The resulting platform demonstrates how existing frameworks can be thoughtfully extended to meet evolving research needs in antenna design while providing evaluation tools for the field.

8.2 Future Scope

In this thesis, I've focused on developing the most essential automation features due to time constraints. Future work could explore:

- **Computational Method Integration:** The current framework relies primarily on FEBI as the default solver method. Incorporating additional computational methods like SBR+ will provide result comparison between solvers, aiding in cases of uncertain reliability.
- **Large-Scale Array Optimization:** One significant limitation was the inability to investigate simulation approaches for arrays with several hundred elements. The underlying research question of determining optimal simulation methods, settings, and simplifications for large-scale arrays remains unaddressed, particularly finding the right balance between speed and accuracy

when dealing with complex coupling effects.

- **Automated Design Optimization:** While the framework can build and analyze predetermined array configurations, it lacks capability for automated optimization where an optimizer could instruct the framework on which models to build and evaluate iteratively.
- **Extended Element Library:** The framework currently supports cross-dipole configurations, but expanding to include other antenna element types like patch antennas or slots would broaden its applicability and address practical limitations encountered when modeling certain array architectures requiring different element geometries.

Bibliography

[1] T. L. Marzetta, E. G. Larsson, H. Yang, and H. Q. Ngo, *Fundamentals of Massive MIMO*, Cambridge, UK: Cambridge University Press, 2016.

[2] A. Sabharwal, P. Schniter, D. Guo, D. W. Bliss, S. Rangarajan, and R. Wichman, "In-band full-duplex wireless: Challenges and opportunities," *IEEE Journal on Selected Areas in Communications*, vol. 32, no. 9, pp. 1637–1652, Sep. 2014.

[3] F. Liu, C. Masouros, A. P. Petropulu, H. Griffiths, and L. Hanzo, "Integrated sensing and communications: Toward dual-functional wireless networks for 6G and beyond," *IEEE Journal on Selected Areas in Communications*, vol. 40, no. 6, pp. 1728–1767, Jun. 2022.

[4] C. A. Balanis, *Antenna Theory: Analysis and Design*, 4th ed., Hoboken, NJ: John Wiley & Sons, 2016.

[5] OpenAI, "AI-generated image illustrating mutual coupling between antennas, generated by ChatGPT in response to user prompt," *ChatGPT*, OpenAI, 2025. [Online]. Available: `https://chat.openai.com/`

[6] R. C. Hansen, *Phased Array Antennas*, 2nd ed., Hoboken, NJ: John Wiley & Sons, 2009.

[7] J.-M. Jin, *The Finite Element Method in Electromagnetics*, 3rd ed., Piscataway, NJ: IEEE Press/Wiley, 2014.

[8] ANSYS Inc., *ANSYS HFSS User Guide*, Release 2024.2, Canonsburg, PA: ANSYS Inc., 2024.

[9] Ansys, Inc., "PyAEDT Documentation," *Ansys Electronics Desktop Python API*, 2024. [Online]. Available: `https://aedt.docs.pyansys.com/`

A

Appendix: Software Configuration and Setup

A.1 Python Library Dependencies

The framework requires the following Python libraries with their primary functions:

- **ansys.aedt.core**
- **plotly**
- **pandas**
- **numpy**
- **scikit-rf**
- **pathlib**
- **json**
- **os, sys**
- **shutil**
- **random**
- **re**

A.2 File Naming Conventions

The framework implements standardized file naming conventions to ensure consistency and traceability:

- **HFSS Project Files:** `[Template_Name], [Array_Dimensions], [Model_Family] - [Random_ID].aedt`
- **Configuration Files:** `[Base_Name], config.json`
- **Data Files:** `[Base_Name], data.json`
- **Touchstone Files:** `[Base_Name], touchstone.s[N]p`
- **Performance Files:** `[Model_Tag]_Simlog.json`

Example complete filename: `Dipole Array, Rev 15_2, 3x3+3x3, AntArr - 8236.aedt`

DEPARTMENT OF SOME SUBJECT OR TECHNOLOGY
CHALMERS UNIVERSITY OF TECHNOLOGY
Gothenburg, Sweden
www.chalmers.se

CHALMERS
UNIVERSITY OF TECHNOLOGY